Journal of Materials Chemistry A

Materials for energy and sustainability

rsc.li/materials-a

ROYAL SOCIETY
OF CHEMISTRY
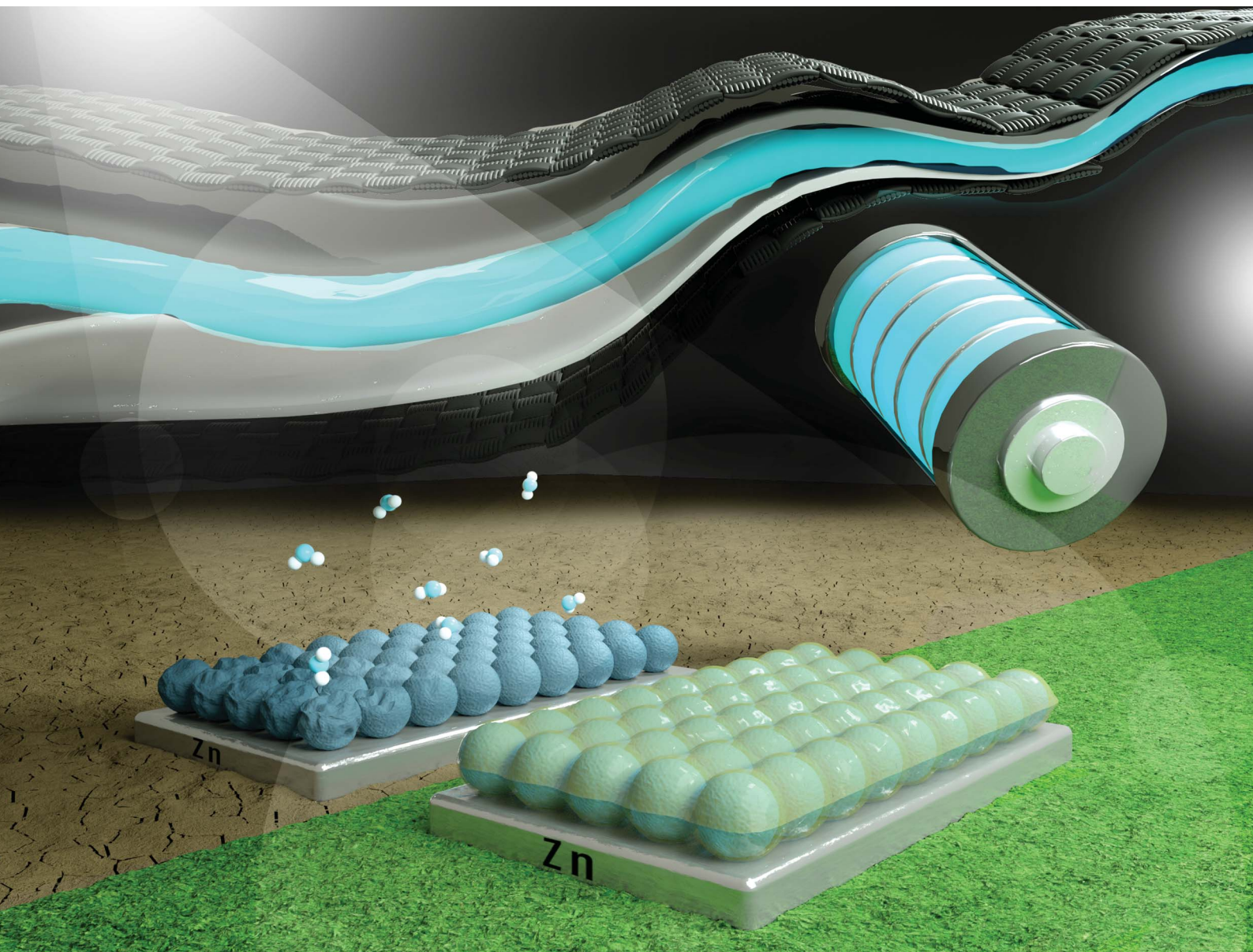
PAPER
Guanjie He, Ivan P. Parkin *et al.*
An anti-aging polymer electrolyte for flexible
rechargeable zinc-ion batteries

PAPER

An anti-aging polymer electrolyte for flexible rechargeable zinc-ion batteries†

Haobo Dong, [a] Jianwei Li, [a] Siyu Zhao, [a] Fangjia Zhao, [a] Siyu Xiong, [a] Dan J. L. Brett, [b] Guanjie He [*abc] and Ivan P. Parkin [*a]

Polymer electrolytes have been extensively applied in zinc-ion batteries, especially those based on hydrogels; however, the densification of the hydrogel electrolytes during cycling affects the durability, resulting in capacity attenuation. It is revealed in this work that the surface electrical resistance of hydrogels is particularly affected by the aging effect. Hence, an adhesive bonding solid polymer electrolyte (ABSPE) for zinc-ion batteries was developed exhibiting significantly enhanced anti-aging properties, where the surface resistance remains constant for over 200 hours, twice that of conventional hydrogel electrolytes. For the hydrogel electrolyte, the surface resistance only remains constant for less than 100 hours which is half of the time achieved by the ABSPE. The ionic conductivity increases with plasticizer loading, reaching 3.77×10^{-4} S cm^{-1}. The kinetic mechanism probed in this work revealed a diffusion-controlled mechanism for Zn/ABSPE/β-MnO$_2$ instead of a capacitive dominated process in the hydrogel electrolyte. In addition, a flexible device was fabricated using a carbon fibre-reinforced polymer composite; this device showed superior power supply performance even under twisting, cutting and bending conditions.

Introduction

Flexible batteries, integrating a constant electrical power supply and physical flexibility, break the constraints of the current rigid battery design and have applications in wearable electronics, roll-up displays and implantable electronics.[1] The liquid electrolytes used in conventional batteries have the challenges of leakage, flammability and mechanical stability that inhibit the development of flexible batteries.[2] Considerable efforts have been made to commercialise thin-film lithium batteries by replacing the liquid electrolyte with ceramic materials such as lithium phosphorus oxynitride (LiPON)[3] and organic polymer electrolytes such as polyethylene oxide (PEO).[4,5] However, their poor ionic conductivity (10^{-4}–10^{-7} S cm^{-1})[6,7] limits the volumetric energy density (100 W h L^{-1}),[8] and stringent fabrication conditions restrict commercialisation.

To date, an alternative strategy, the flexible zinc-ion batteries (ZIBs), have attracted considerable interest owing to the high specific capacity of zinc (5855 mA h cm^{-3}),[9,10] inherently superior safety characteristics and the availability of robust manufacturing methods. Attributed to the pioneering work in rechargeable aqueous zinc-ion batteries (AZIBs),[11–17] hydrogel electrolytes have been developed that combine the benefits of aqueous electrolytes with the flexibility offered by polymers. Zhi[18–20] and co-workers made a significant contribution in evaluating ionic conductivities of hydrogel polymer electrolytes (HPEs) and integrating additional functionalities such as anti-freezing[21] and self-healing[22] abilities. As summarised in Table S1,† the average ionic conductivity of solid polymer electrolytes is around 10^{-5} S cm^{-1}, and the hydrogel polymer electrolyte based on a polyacrylamide (PAM) framework even achieves 10^{-2} S cm^{-1} with a similar specific capacity to AZIBs (306 mA h g^{-1}). Moreover, the water molecules that existed in the hydrogel electrolyte enhance the contact of the solid–solid interface between the electrodes and electrolyte, resulting in continuous chemical reactions through the interface. While these results are very promising, there remain challenges associated with aging of the hydrogel electrolyte that leads to performance degradation. As such, 'anti-aging' properties need to be integrated into this component to achieve a viable commercial offering. In addition, Zhi *et al.* have noticed the side effect of induced hydrogen evolution reaction (HER) in the aqueous system and hence developed hydrogen-free and dendrite-free all-solid-state zinc ion batteries by complexing ionic liquid 1-ethyl-3-methyl-imidazolium tetrafluoroborate ([EMIM]BF$_4$) with 2 M zinc tetrafluoroborate (Zn(BF4)$_2$) into the polymer matrix poly(vinylidene fluoride-hexafluoropropylene) (PVDF-HFP).[23] Assembled with the cobalt hexacyanoferrate

aChristopher Ingold Laboratory, Department of Chemistry, University College London, 20 Gordon Street, London WC1H 0AJ, UK. E-mail: g.he@ucl.ac.uk; i.p.parkin@ucl.ac.uk

bElectrochemical Innovation Lab, Department of Chemical Engineering, University College London, 20 Gordon Street, London WC1H 0AJ, UK

cSchool of Chemistry, University of Lincoln, Brayford Pool, Lincoln, LN6 7TS, UK

† Electronic supplementary information (ESI) available. See DOI: 10.1039/d0ta07086f

This journal is © The Royal Society of Chemistry 2020

J. Mater. Chem. A, 2020, **8**, 22637–22644 | **22637**

cathode, the as-fabricated solid state zinc-ion batteries delivered a stable cycling capability with nearly 100% coulombic efficiency.

For hydrogel electrolytes, a higher ionic conductivity requires a greater amount of aqueous electrolyte absorbed in the porous polymer framework. The more water molecules absorbed, the greater the free volume provided for the segmental motion of Zn^{2+} in the quasi-solid-state electrolyte. However, the evaporation of water from the hydrogel densifies the electrolyte during cycling, resulting in increasing internal resistance and capacity loss.

In this work, an adhesive bonding solid polymer electrolyte (ABSPE) was developed for zinc-ion batteries by combining a polymer framework (poly(ethylene glycol)diglycidylether (PEGDGE)), a zinc-ion salt (zinc trifluoromethanesulfonate (ZnOTf)) and a plasticizer (propylene carbonate (PC)). Owing to the presence of hydroxyl groups and the aromatic rings in the diglycidylether, interfacial contact could be enhanced by the adhesive bonding between the solid–solid interface *via* attractive interactions, largely avoiding the aging issue in hydrogel electrolytes. Hydroxyl groups (–OH) formed in the polymerisation induce bond formations or strong polar attractions to oxide or hydroxyl surfaces. The as-fabricated solid polymer electrolyte exhibits an ionic conductivity of 3.77×10^{-4} S cm^{-1} and excellent aging stability, maintaining a constant surface resistance (R_f) for at least 200 hours, examined using periodic electrochemical impedance spectroscopy (EIS) testing. Using carbon cloth as the substrate for commercial electrodes based on β-MnO_2 and zinc powder, the as-assembled battery can be regarded as a carbon fibre-reinforced polymer composite capable of delivering constant power under various physical deformations.

Results and discussion

The adhesive bonding solid polymer electrolyte was synthesised based on an epoxy-based thermosetting polymer poly(ethylene glycol)diglycidylether (PEGDGE, $M_n = 500$) as shown in the schematic diagram (Fig. 1a) by free radical polymerisation. A zinc-ion salt, zinc trifluoromethanesulfonate (Zn(OTf), ≥98%), was dissolved into the polymer framework PEGDGE, stirring for at least 3 hours until a homogeneous transparent solution was obtained. Afterwards, the curing agent triethylenetetramine (TETA, ≥97%), an aliphatic amine, was added into the complexe in the molar ratio of 1 : 4 (TETA : PEGDGE). Propylene carbonate (PC, anhydrous), a common organic solvent for ionic salts, was also added into the solution. Since the maximum solvability for ZnOTf in PC is 0.04 mol L^{-1} (ref. 24), PC is regarded as a filler, expanding the free volume for ionic transportation. To address the relation between ionic conductivity and the plasticizer in zinc-ion batteries, ABSPEs with various quantities of PC were fabricated. Differential scanning calorimetry (DSC) was applied to determine the polymerisation curing temperature (see Fig. S1†). All chemicals were supplied from Sigma-Aldrich UK and the experimental details are in the ESI.† PEGDGE and TETA were polymerised by free radical polymerisation, in which the diglycidylether ring of PEGDGE opens and reacts with two primary amino groups in TETA, as shown in Fig. S2.† The polymerisation mechanism of the epoxide ring opening process was also evaluated by Raman spectroscopy analysis (Fig. S10†). Compared to pure PEGDGE, the missing peaks centered at 1256 cm^{-1} and 1133 cm^{-1} belong to the epoxide ring deformation,[25] while the missing peak at 912 cm^{-1} corresponded to an epoxide ring breathing-mode.[25] The polymer film exhibits a light brown color, as shown in
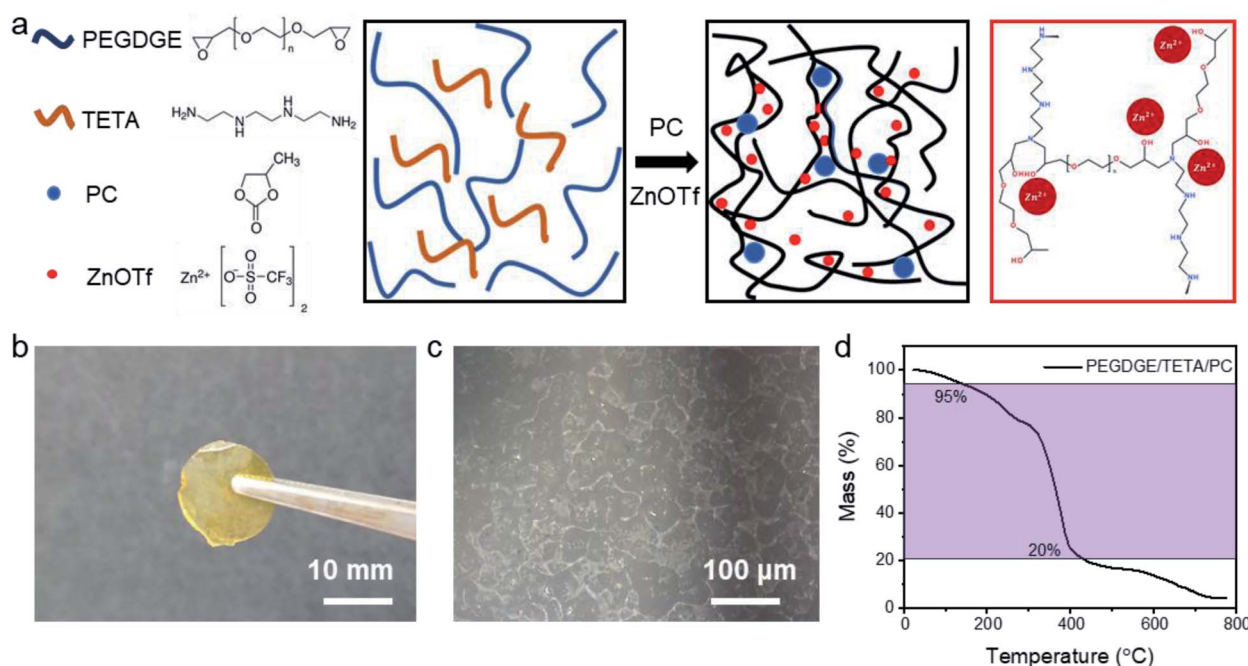

Fig. 1 (a) Schematic diagram of the synthesis process for the polymer electrolyte; (b) optical image of the polymer electrolyte film PEGDGE/TETA/PC/ZnOTf; (c) optical microscopy image of the polymer electrolyte; (d) TGA of the polymer electrolyte.

22638 | J. Mater. Chem. A, 2020, 8, 22637–22644

This journal is © The Royal Society of Chemistry 2020

Fig. 1b. Due to the low contrast, the structure is characterized by optical microscopy (Fig. 1c), where the crystalline zones observed are located in the amorphous background with a transparent structure.[26] The as-fabricated solid polymer electrolyte is homogeneous as shown by the Energy-dispersive X-ray spectroscopy (EDX) mapping images (Fig. S3†). As shown in Fig. 1d, good thermal stability of the polymer electrolyte was obtained, for which rapid degradation occurred at 313 °C. The 5% weight loss observed at 119 °C is likely caused by the loss of the PC.

Although the zinc ion transfer mechanism in the polymer electrolyte has not been fully investigated, a reasonable ion mechanism could be deduced, according to the detailed observation in the lithium-ion gel polymer. There is general agreement that ion transmission happens by the segmental motion of the small chains in the amorphous region of the polymer host.[27,28] When ZnOTf is added, PEGDGE with sequential polar groups, such as –O– and C–N, dissolves the zinc salts and form polymer–salt complexes, as shown in Fig. 1a. As to further increase the content of the amorphous phase, the plasticizer PC, was used because of its low glass transition temperature and high dielectric constant. Incorporating the polymer host with low molecular weight compounds, the intermolecular and intramolecular forces between the polymer chains are reduced, consequently reducing the rigidity of the three-dimensional structure.[27,29,30] As a common organic solvent, only 0.04 mol L^{-1} ZnOTf can be dissolved in PC;[24] hence, PC is regarded as a low-molar-mass filler impeding chain folding and increasing free volume and speed segmental relaxation.[7,31]

The X-ray powder diffraction (XRD) pattern for the polymer electrolyte (Fig. 2a) showed incoherent broad scattering around 10° that demonstrates that most regions of the polymer are in the amorphous phase. The amorphous phase enables Zn^{2+} ion transport through the polymer electrolyte to the electrodes. The crosslinking mechanism has also been verified
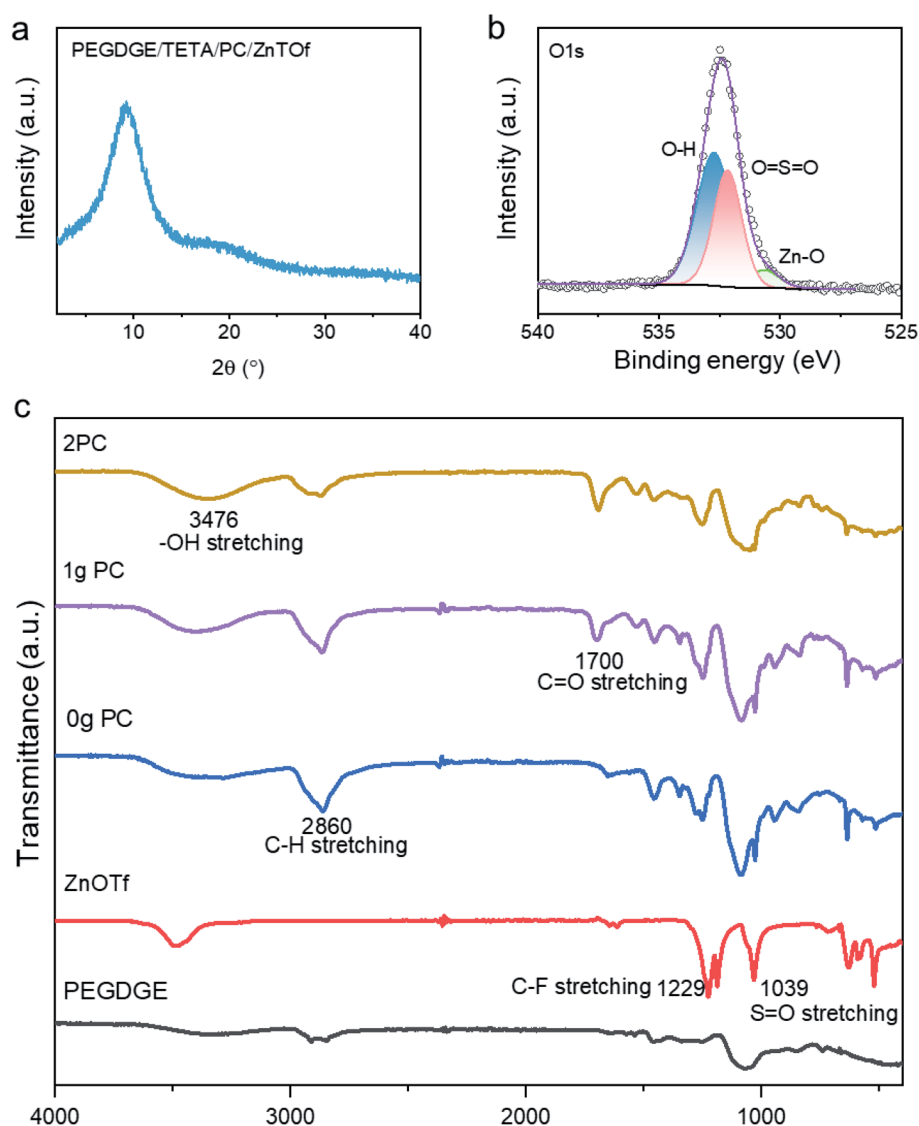

Fig. 2 (a) XRD pattern for PEGDGE/TETA/PC/ZnOTf; (b) XPS spectra for O 1s; (c) FTIR spectrum of ABSPEs with different amounts of PC.

This journal is © The Royal Society of Chemistry 2020

J. Mater. Chem. A, 2020, **8**, 22637–22644 | **22639**

by X-ray photoelectron spectroscopy (XPS), where the hypothesis of zinc ion transportation has also been confirmed. As displayed in the spectra for O 1s (Fig. 2b), the presence of the ionic bond of Zn–O at a binding energy of 530.5 eV proves that zinc ions will couple with the oxygen in the free hydroxylic groups, hopping to the neighbouring sites. Spectra for Zn 2p, shown in Fig. S8d,† also reveal that Zn–O has a binding energy of 1045 eV. In the conventional 2p spectra, the area enclosed by Zn $2p_{1/2}$ and S $2p_{1/2}$ is half that of the area enclosed by Zn $2P_{3/2}$ and S $2P_{3/2}$, respectively. Fourier-transform infrared spectroscopy (FTIR) (see Fig. 2c) was used to elucidate the polymerisation mechanism of the polymer. In the background spectrum of ZnOTf, C–F groups and S=O groups are observed at 1229 cm^{-1} and 1039 cm^{-1}, respectively. Focusing on the polymer with PC, there is an additional band at 1700 cm^{-1} compared to the polymer without PC, which is due to the stretching of C=O. The peak at 1095 cm^{-1} is in the region for C–O stretching in the polymer PEGDGE. Hydroxyl groups –OH formed during the crosslinking between PEGDGE and aliphatic amine are observed at *ca.* 3476 cm^{-1}, related to free non-hydrogen bonded groups. The majority of zinc cations are bonded with free-electron donors, –OH, forming coordinated

bonds, while the addition of plasticizer PC offers C=O free groups to form polymer–salt complexes. As displayed in Fig. 1a, the transportation of zinc ions in the polymer is amenable to segmental motion.

The solid-state ZIBs for electrochemical tests were assembled in a coin cell (CR2032) under open-air conditions with a zinc foil anode, fabricated β-MnO$_2$ cathode, and the solid electrolyte ABSPE. The cathode was fabricated by casting the commercial active cathode material, β-MnO$_2$ onto the carbon paper before assembling in the sandwich structure. The cyclic voltammograms (CV) (Fig. 3a) investigated under scan rates of 0.5 mV s^{-1} to 5 mV s^{-1}, from 0.8 V to 2.0 V, exhibit a reduction peak and oxidation peak located at 1.69 V and 1.21 V at a scan rate of 1 mV s^{-1}, respectively. The redox peaks were assigned to the change of the valence state for Mn in β-MnO$_2$ from Mn^{4+} to Mn^{3+} at 1.69 V accompanying the redox reaction of Zn to Zn^{2+} at the anode. To further understand the kinetic process for the epoxy-based solid-state ZIBs, diffusion-controlled and capacitive contribution to performance (Fig. 3b and c) were analysed based on the following relations:[32]
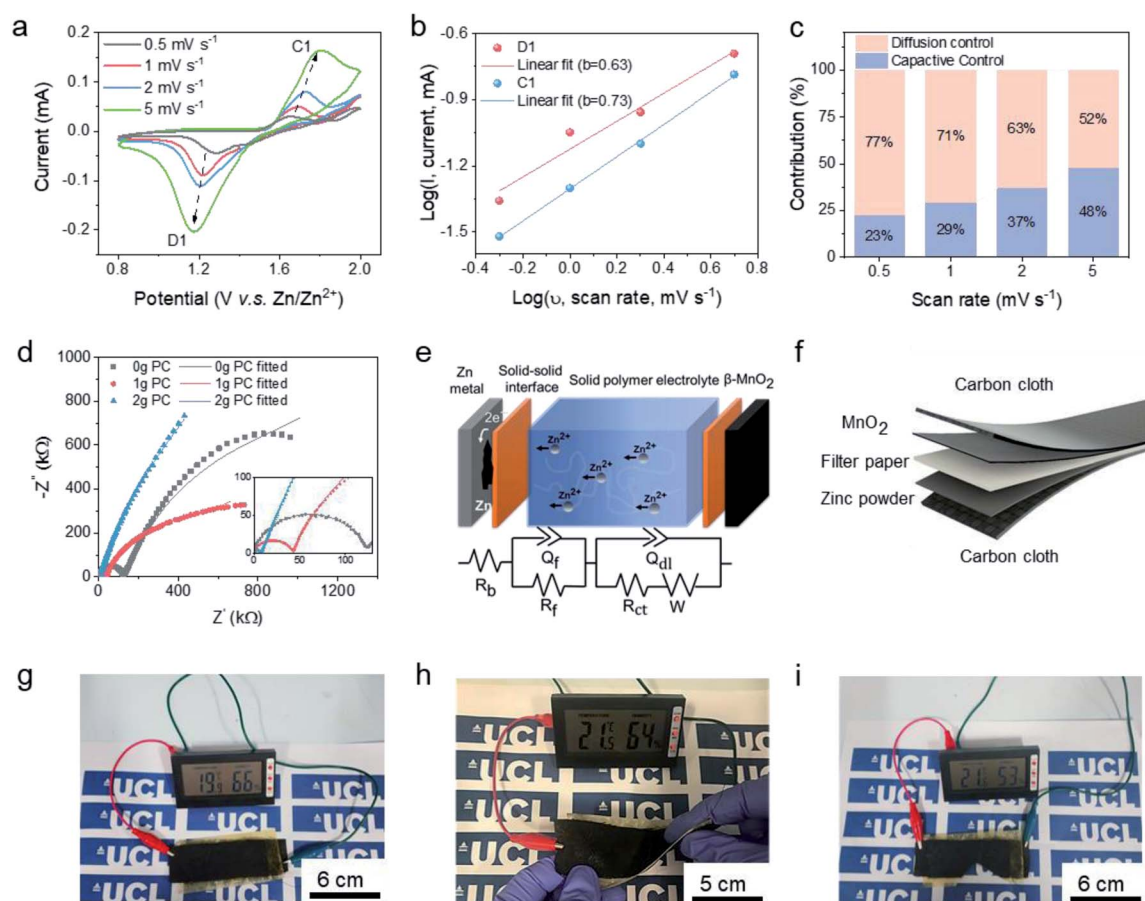
$$i = av^b$$

Fig. 3 (a) CV curves for Zn/ABSPE/β-MnO$_2$ at scan rates 0.5, 1, 2, and 5 mV s^{-1}; (b) diffusion–capacitive contribution with log(i) *vs.* log(v) plots for two peaks C1 and D1 in CV curves; (c) diffusion–capacitive control contribution presented in the bar chart; (d) EIS plots of Zn/ABSPE/β-MnO$_2$ in different amounts of PC; (e) EIS equivalent circuit; (f) flexible device configuration; (g) flexible device powering a digital temperature–humidity meter; (h) twisting the device; (i) cutting the device.

22640 | *J. Mater. Chem. A*, 2020, **8**, 22637–22644

This journal is © The Royal Society of Chemistry 2020

Hence,

$$\log(i) = \log(a) + b\log(v)$$

where i refers to the peak current and v is the scan rate. a and b interpreted from the log–log plot (Fig. 3b) are variables related to the diffusion-controlled and capacitive contribution; where, if b is close to 0.5 the kinetic process is mainly influenced by diffusion control, otherwise, if b is close to 1, a capacitive process is dominating. The b values for redox peaks C1 and D1 are 0.73 and 0.63, respectively, indicating the kinetic process is mainly diffusion-controlled, rather than under capacitive control. A detailed estimation of diffusion and capacitive contributions is shown in Fig. 3c which further reveals that the electrochemical reaction is dominated by ionic diffusion; whereas as the scan rate is increased, there is an increasing proportion of pseudocapacitance, reaching 48% at a scan rate of 5 mV s^{-1}. The ionic conductivities for Zn/ABSPE/β-MnO$_2$ were determined by electrochemical impedance spectroscopy (EIS) for the polymer electrolytes with varying amounts of PC. Focusing on Nyquist plots (see Fig. 3d), the two semi-circles attained reveal the equivalent resistance series (ESR) consisting of a bulk resistance (R_b), a surface resistance (R_f) and a charge transfer resistance (R_{ct}) as displayed in Fig. 3e. Ionic conductivities, summarised in Table S2,† were calculated based on R_b. As displayed in Fig. S9a,† the ionic conductivity increases with plasticizer (PC) content, reaching 3.77×10^{-4} S cm^{-1}, which correlates with the hypothesis that the free volumes are expanded by PC for the segmental motion of Zn^{2+}, resulting in higher ionic conductivity. However, there is a decrease in ionic conductivity over an optimal concentration ratio of PC (56 wt%). When PC is over 50 wt% in the polymer electrolyte, the lower amounts of ZnOTf (Fig. S9b†) result in a slight reduction in ionic conductivity. As shown in Fig. S13a,† the as-prepared solid-state Zn/β-MnO$_2$ battery exhibits a specific capacity of 177 mA h g^{-1} at a current density of 0.1 A g^{-1}, even at 2 A g^{-1} it can deliver a specific capacity of 47 mA h g^{-1}. The charge/discharge rate performance (Fig. S13b†) exhibits two typical voltage plateaus at 1.7 V and 1.2 V, which are consistent with the two pairs of redox peaks in the CV curves (Fig. 3a). Meanwhile, it also exhibits a stable cycling ability at 0.5 A g^{-1}, for which there is a 100% coulombic efficiency with a capacity retention of 85% after 300 cycles.

A flexible device referred to as a carbon fibre-reinforced polymer composite was fabricated in a sandwich structure with the substrate carbon cloth acting as the electrodes. As shown in Fig. 3f, a glass fibre mat was applied in the middle of the stack to avoid short-circuiting and improve the mechanical properties. The entire device was manufactured by the vacuum resin molding strategy, as shown in Fig. S7.† The as-fabricated flexible device can power a temperature-humanity meter (see Fig. 3g) as an indicator of continuous operation. As a flexible device, it can still generate power during twisting, bending and even cutting, as shown in Fig. 3h and i, respectively. Moreover, as revealed in Fig. S13d,† under the deformation, the device still exhibits a high coulombic efficiency above 95% at a current density of 2 A g^{-1}.

Owing to the absence of water molecules in the polymer electrolyte, the ionic diffusion in ABSPE exhibits a wider electrochemical stability window, as shown in Fig. S5,† where a symmetric Zn/ABSPE/Zn cell was tested. Scanning the potential over the range −3 to 3 V, zinc plating was detected at ±1.9 V during the first cycle. Due to the irreversible zinc deposition at the surface of the electrodes (see Fig. S3†), the potential window was reduced to ±1.2 V for the second cycle, coupled with a reduction in the peak current. The presence of the cathodic and anodic peaks is related to the reversible reaction of the polymer electrolyte ABSPE in which Zn $\leftrightarrow$ Zn^{2+} + 2e$^-$. Generally, zinc stripping/deposition for aqueous and hydrogel ZIBs occurs at ±0.3 V in symmetric cells; the large operational voltage window (−1.9 V to 1.9 V) for ABSPE is beneficial for ZIBs to achieve high voltage, avoiding the hydrogen evolution reaction (HER) at the cathode.

The aging stability of the polymer electrolytes (see Fig. 4a) was investigated by recording the EIS spectra every 10 hours for 400 hours under ambient conditions so as to simulate under realistic working scenarios. As shown in Fig. 4b, R_b remains constant at ~200 Ω through the 400 hours test, while R_f remains constant at ~2000 Ω for ~200 hours. The smoothed curve for R_f indicates a substantial increase, nearly an exponential growth, in surface resistance after 200 hours. For comparison, the aging effect for a conventional alginate hydrogel electrolyte was also investigated (see Fig. 4c). As displayed in Fig. 4d, R_b of the hydrogel electrolyte remains constant at ~6 Ω for 170 hours; however, the resistance subsequently jumps to 20 Ω. R_f remains constant around 300 Ω for 100 hours followed by an exponential increase, as observed for ABSPE. For both ABSPE and HPE, the good stability of the internal resistance reveals that the ion transportations in the pristine polymer electrolyte are less influenced by the aging effect, whereas surface resistances are more sensitive to aging issues. The different phenomena of ABSPE and HPE in bulk resistance could be explained by the thermal stability. As the ionic conductivity for HPE generally increases with higher water content,[33–35] the densification of HPE itself induced by the evaporation of the water molecules will result in lower ionic conductivity and hence a greater bulk resistance. TGA results for HPE (Fig. S11†) also prove the thermal stability where the degradation temperature for HPE is below 100 °C compared to 313 °C for ABSPE as shown in Fig. 1d.

The attenuation of ion transmission at the electrode–polymer interface could be ascribed to the densification of the polymer at the surface and the growth of zinc deposits on the anode. Densification was identified as the primary reason and is induced by solvent evaporation, such as water for HPEs and PC in ABSPEs, which reduces the surface wettability between electrodes and electrolyte; hence, surface resistances are likely to be influenced by the aging effect. Compared with HPEs, epoxy-based polymer electrolytes exhibit relatively high stability in R_f. Owing to the diglycidyl ether groups in the ABSPEs, hydroxylic groups and amine groups formed after the ring-opening reaction[36] generate a strong intermolecular bond and hydrogen bond at the interface,[37] which restricts the evaporation of the PC solvent. As reported by Fourche,[38]

This journal is © The Royal Society of Chemistry 2020
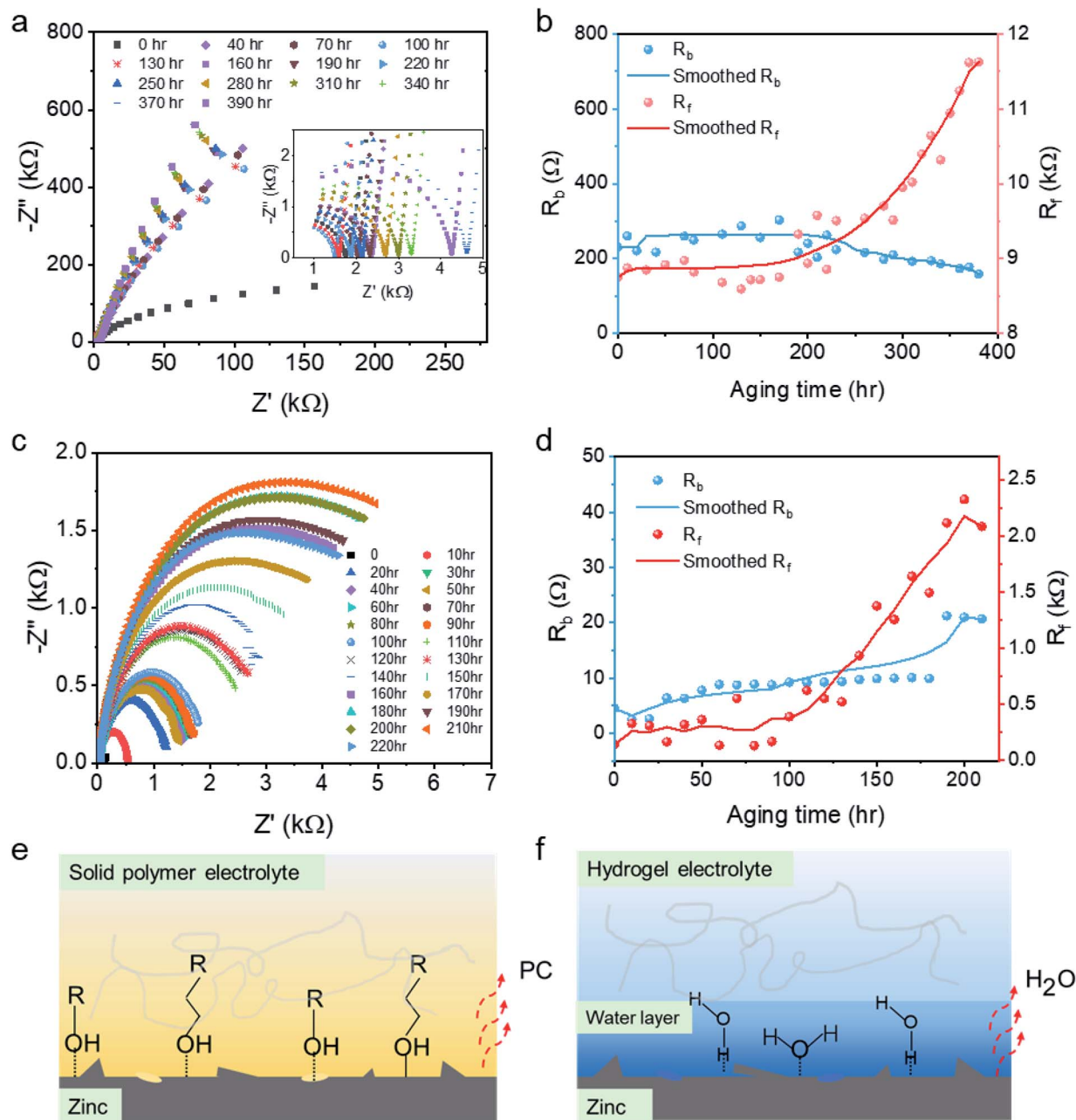
J. Mater. Chem. A, 2020, 8, 22637–22644 | 22641

Fig. 4 (a) EIS aging test for ABSPE (Zn/ABSPE/Zn); (b) bulk and surface resistances for ABSPE; (c) EIS aging test for alginate hydrogel polymer electrolyte (Zn/HPE/Zn); (d) bulk and surface resistances for alginate hydrogel polymer electrolyte; (e) surface intermolecular forces for ABSPEs; (f) surface intermolecular forces for HPEs.

chemical bonding takes place extensively in the case of polymer–metal interfaces; moreover, metal–polymer adsorption bonds (M–O–C) are observed for metals such as Al, Fe and Ni coated with epoxy.[39] Therefore, the covalent bonds (Zn–O–C) shown in Fig. 4e could form for ABSPEs under the Lewis acid–base reactions activated by the interfacial electrical field.[40] The metal–polymer adsorption bonds strongly stabilise the interface, avoiding the aging effect. For HPEs, water molecules present on the surface of the hydrogel enhance the wettability for ionic diffusion, whereas the intermolecular coulombic forces are lost as a result of the ingress of media with a high dielectric constant, such as water[41] (see Fig. 4f). Because of the greater evaporation rate of water (BuAc = 0.3 (ref. 42)) compared with PC (BuAc = 0.005 (ref. 43)), free dissociated water molecules absorbed in the HPEs, interacting *via* dipole–dipole forces, are easily lost, resulting in a shorter aging time. Nazarov,[40] who also investigated a zinc/epoxy interface, indicated that water adsorption and desorption rapidly changed the potential drop across the zinc/polymer interface. The potential variation during water drying and restoration processes reflect the sensitive change in the surface resistances.

22642 | J. Mater. Chem. A, 2020, 8, 22637–22644

This journal is © The Royal Society of Chemistry 2020

Conclusions

In summary, an adhesive bonding solid polymer electrolyte was developed for rechargeable zinc-ion batteries and exhibited excellent anti-aging properties and a large electrochemical window. With an increasing amount of the plasticizer (PC), the ionic conductivity could be increased to 3.77×10^{-4} S cm^{-1}. The carbon fibre reinforced polymer composite fabricated by VARTM provides a reliable power supply under bending, twisting and cutting. In relation to the aging effect, it is obvious that the surface resistance is more sensitive for both polymer and hydrogel electrolytes compared to the polymer bulk resistance. Interface intermolecular interactions and densification of the solvent were identified as the explanation for the attenuation in capacity during cycling at the interface.

Conflicts of interest

There are no conflicts to declare.

Acknowledgements

References

1 L. Mao, Q. Meng, A. Ahmad and Z. Wei, *Adv. Energy Mater.*, 2017, **7**, 1–19.

2 W. Liu, M. S. Song, B. Kong and Y. Cui, *Adv. Mater.*, 2017, **29**, 1603436.

3 J. B. Bates, N. J. Dudney, B. Neudecker, A. Ueda and C. D. Evans, *Solid State Ionics*, 2000, **135**, 33–45.

4 Y. Liu, S. Gorgutsa, C. Santato and M. Skorobogatiy, *J. Electrochem. Soc.*, 2012, **159**, A349–A356.

5 O. Borodin and G. D. Smith, *Macromolecules*, 2006, **39**, 1620–1629.

6 A. Manthiram, X. Yu and S. Wang, *Nat. Rev. Mater.*, 2017, **2**, 1–16.

7 T. Kim, W. Song, D. Y. Son, L. K. Ono and Y. Qi, *J. Mater. Chem. A*, 2019, **7**, 2942–2964.

8 G. Zhou, F. Li and H. M. Cheng, *Energy Environ. Sci.*, 2014, **7**, 1307–1338.

9 D. Selvakumaran, A. Pan, S. Liang and G. Cao, *J. Mater. Chem. A*, 2019, **7**, 18209–18236.

10 M. Song, H. Tan, D. Chao and H. J. Fan, *Adv. Funct. Mater.*, 2018, **28**, 1–27.

11 H. Pan, Y. Shao, P. Yan, Y. Cheng, K. S. Han, Z. Nie, C. Wang, J. Yang, X. Li, P. Bhattacharya, K. T. Mueller and J. Liu, *Nat. Energy*, 2016, **1**, 1–7.

12 J. Li, K. McColl, X. Lu, S. Sathasivam, H. Dong, L. Kang, Z. Li, S. Zhao, A. G. Kafizas, R. Wang, D. J. L. Brett, P. R. Shearing, F. Corà, G. He, C. J. Carmalt and I. P. Parkin, *Adv. Energy Mater.*, 2020, **10**, 1–14.

13 D. Kundu, B. D. Adams, V. Duffort, S. H. Vajargah and L. F. Nazar, *Nat. Energy*, 2016, **1**, 1–8.

14 N. Zhang, F. Cheng, J. Liu, L. Wang, X. Long, X. Liu, F. Li and J. Chen, *Nat. Commun.*, 2017, **8**, 1–9.

15 L. Ma, S. Chen, C. Long, X. Li, Y. Zhao, Z. Liu, Z. Huang, B. Dong, J. A. Zapien and C. Zhi, *Adv. Energy Mater.*, 2019, **9**, 1–10.

16 P. He, G. Zhang, X. Liao, M. Yan, X. Xu, Q. An, J. Liu and L. Mai, *Adv. Energy Mater.*, 2018, **8**, 1–6.

17 B. Tang, L. Shan, S. Liang and J. Zhou, *Energy Environ. Sci.*, 2019, **12**, 3288–3304.

18 H. Li, C. Han, Y. Huang, Y. Huang, M. Zhu, Z. Pei, Q. Xue, Z. Wang, Z. Liu, Z. Tang, Y. Wang, F. Kang, B. Li and C. Zhi, *Energy Environ. Sci.*, 2018, **11**, 941–951.

19 Y. Huang, J. Liu, J. Zhang, S. Jin, Y. Jiang, S. Zhang, Z. Li, C. Zhi, G. Du and H. Zhou, *RSC Adv.*, 2019, **9**, 16313–16319.

20 H. Li, Z. Liu, G. Liang, Y. Huang, Y. Huang, M. Zhu, Z. Pei, Q. Xue, Z. Tang, Y. Wang, B. Li and C. Zhi, *ACS Nano*, 2018, **12**, 3140–3148.

21 F. Mo, G. Liang, Q. Meng, Z. Liu, H. Li, J. Fan and C. Zhi, *Energy Environ. Sci.*, 2019, **12**, 706–715.

22 D. Wang, L. Wang, G. Liang, H. Li, Z. Liu, Z. Tang, J. Liang and C. Zhi, *ACS Nano*, 2019, **13**, 10643–10652.

23 L. Ma, S. Chen, N. Li, Z. Liu, Z. Tang, J. A. Zapien, S. Chen, J. Fan and C. Zhi, *Adv. Mater.*, 2020, **32**, 1908121.

24 J. J. Xu, H. Ye and J. Huang, *ECS Meet. Abstr.*, 2006, vol. MA2005-01, p. 116.

25 J. R. Nair, I. Shaji, N. Ehteshami, A. Thum, Di. Diddens, A. Heuer and M. Winter, *Chem. Mater.*, 2019, **31**, 3118–3133.

26 C. Ma, K. Dai, H. Hou, X. Ji, L. Chen, D. G. Ivey and W. Wei, *Adv. Sci.*, 2018, **5**, 1–9.

27 S. B. Aziz, T. J. Woo, M. F. Z. Kadir and H. M. Ahmed, *J. Sci. Adv. Mater. Devices*, 2018, **3**, 1–17.

28 L. Long, S. Wang, M. Xiao and Y. Meng, *J. Mater. Chem. A*, 2016, **4**, 10038–10039.

29 Z. Xue, D. He and X. Xie, *J. Mater. Chem. A*, 2015, **3**, 19218–19253.

30 M. Armand, *Nature*, 2001, **414**, 359–367.

31 Y. T. Kim and E. S. Smotkin, *Solid State Ionics*, 2002, **149**, 29–37.

32 G. He, M. Qiao, W. Li, Y. Lu, T. Zhao, R. Zou, B. Li, J. A. Darr, J. Hu, M. M. Titirici and I. P. Parkin, *Adv. Sci.*, 2017, **4**, 1600214.

33 M. Z. Kufian, S. R. Majid and A. K. Arof, *Ionics*, 2007, **13**, 231–234.

34 Y. Huang, M. Zhong, Y. Huang, M. Zhu, Z. Pei, Z. Wang, Q. Xue, X. Xie and C. Zhi, *Nat. Commun.*, 2015, **6**, 1–8.

35 C. J. Lee, H. Wu, Y. Hu, M. Young, H. Wang, D. Lynch, F. Xu, H. Cong and G. Cheng, *ACS Appl. Mater. Interfaces*, 2018, **10**, 5845–5852.

36 N. T. Nguyen, A. H. Milani, J. Jennings, D. J. Adlam, A. J. Freemont, J. A. Hoyland and B. R. Saunders, *Nanoscale*, 2019, **11**, 7921–7930.

37 J. H. Lee, S. G. Kang, Y. Choe and S. G. Lee, *Compos. Sci. Technol.*, 2016, **126**, 9–16.

38 G. Fourche, *Polym. Eng. Sci.*, 1995, **35**, 957–967.

This journal is © The Royal Society of Chemistry 2020

J. Mater. Chem. A, 2020, **8**, 22637–22644 | **22643**

39 T. Duguet, A. Gavrielides, J. Esvan, T. Mineva and C. Lacaze-Dufaure, *J. Phys. Chem. C*, 2019, **123**, 30917–30925.

40 A. Nazarov, T. Prosek and D. Thierry, *Electrochim. Acta*, 2008, **53**, 7531–7538.

41 A. S. Vol'mir, *Strength Mater.*, 1978, **10**, 1375–1376.

42 *The MSDS HyperGlossary: Evaporation Rate*, http://www.ilpi.com/msds/ref/evaporationrate.html, accessed 14 May 2020.

43 *Technical report of propylene carbonate*, https://www.lyondellbasell.com/globalassets/documents/chemicals-technical-literature/lyondellbasell-chemicals-technicalliterature-propylene-carbonate-2417.pdf, accessed 14 May 2020.